ORNL/TM-2020/1820

Post Irradiation Examination of Candidate NpO_2 Targets for ^{238}Pu Production

R. N. Morris
T. Jordan
P. L. Mulligan

March 2021

OAK RIDGE NATIONAL LABORATORY
MANAGED BY UT-BATTELLE FOR THE US DEPARTMENT OF ENERGY

ORNL/TM-2020/1820

Nuclear Energy and Fuel Cycle Division

POST EXAMINATION OF CANDIDATE NpO_2 TARGETS FOR ^{238}Pu PRODUCTION

R. N. Morris
T. Jordan
P. L. Mulligan

March 2021

Prepared by
OAK RIDGE NATIONAL LABORATORY
Oak Ridge, TN 37831-6283
managed by
UT-BATTELLE, LLC
for the
US DEPARTMENT OF ENERGY
under contract DE-AC05-00OR22725

CONTENTS

LIST OF FIGURES

LIST OF TABLES

ACRONYMS AND ABBREVIATIONS

CERMET	ceramic–metallic
DLL	dynamic-link library
EOC	end of cycle
FEA	finite element analysis
HFIR	High Flux Isotope Reactor
ID	inner diameter
LOCA	loss-of-coolant accident
MET	metallography
OD	outer diameter
ORNL	Oak Ridge National Laboratory
REDC	Radiochemical Engineering Development Center

ABSTRACT

Four targets composed of sintered NpO_2 pellets enclosed in Zircaloy cladding were irradiated in the High Flux Isotope Reactor for 2 to 4 cycles to determine if an oxide pellet and Zircaloy cladding would be usable candidates for ^{238}Pu production. The pellets were sintered to a high fraction of theoretical density (TD) and melt wires were placed in small holes that had been drilled in the center of selected pellets to determine if the pellet centers exceeded desirable operating temperatures. After irradiation, the targets were punctured to determine the internal target pressure and the fission gas release. None of the targets had excessive pressure and fission gas release was in the range of 4 to 38%. The targets were then cut into segments for radiochemical analysis, and metallographic (MET) mounts were created to examine the pellet microstructure and to search for the melt wires to determine if they had melted. Three of the four targets resulted in successful MET mounts; the two-cycle pellets were too friable to be handled. No signs of pellet melting were noted, and unfortunately, none of the melt wires could be recovered. The results indicate that this pellet/clad design offers a practical option for ^{238}Pu production.

1. TARGET DESCRIPTION

1.1 INTRODUCTION

Oak Ridge National Laboratory (ORNL) is currently resuming production of ^{238}Pu after a nationwide hiatus of many decades. The primary option has been a ceramic–metallic (CERMET) pellet composed of powdered aluminum and NpO_2 which is pressed and sintered into pellets at low temperature, after which the pellets are loaded into an aluminum cladding target [1] which is hydrostatically compressed down onto the pellets to ensure sufficient heat transfer. While this design is suitable for the task, to increase NpO_2 loading a design using a single component pellet is desired and there is also a need for fewer targets and less complex processing to recover the ^{238}Pu. With this in mind, a target consisting of NpO_2 pellets in a Zircaloy cladding has been developed.

Because of the uncertainties in the neutron capture cross section for ^{237}Np and thermophysical properties of irradiated NpO_2, there was a concern that the pellets could melt near their centerline sometime during a 2–4 cycle irradiation in the High Flux Isotope Reactor (HFIR). To avoid possible reactor safety issues, four NpO_2 pellets were sandwiched between hafnia pellets to suppress neutron flux on either end of the pellet stack, mitigating fission peaking in the top and bottom pellets. Additional precautions were taken to accommodate possible NpO_2 melting by placing refractory metal tungsten crucibles above and below the pellet stack. Highly absorbing hafnium metal cylinders were placed over the tungsten crucibles to prevent further fissioning of NpO_2 material if the pellets were to melt into these regions. Finally, this assembly was placed into an aluminum capsule as a secondary containment. The design also included a semicircular hafnium shield to simulate the neutron flux self-shielding caused by additional NpO_2 targets anticipated in the future production design. See Figure 1.

Melt wires were placed in the centers of two of the pellets to serve as temperature indicators. One of these assemblies was irradiated for 2 cycles, two were irradiated for 3 cycles, and one was irradiated for 4 cycles. After irradiation, the targets were transferred to Building 3525 for post irradiation examination (PIE).

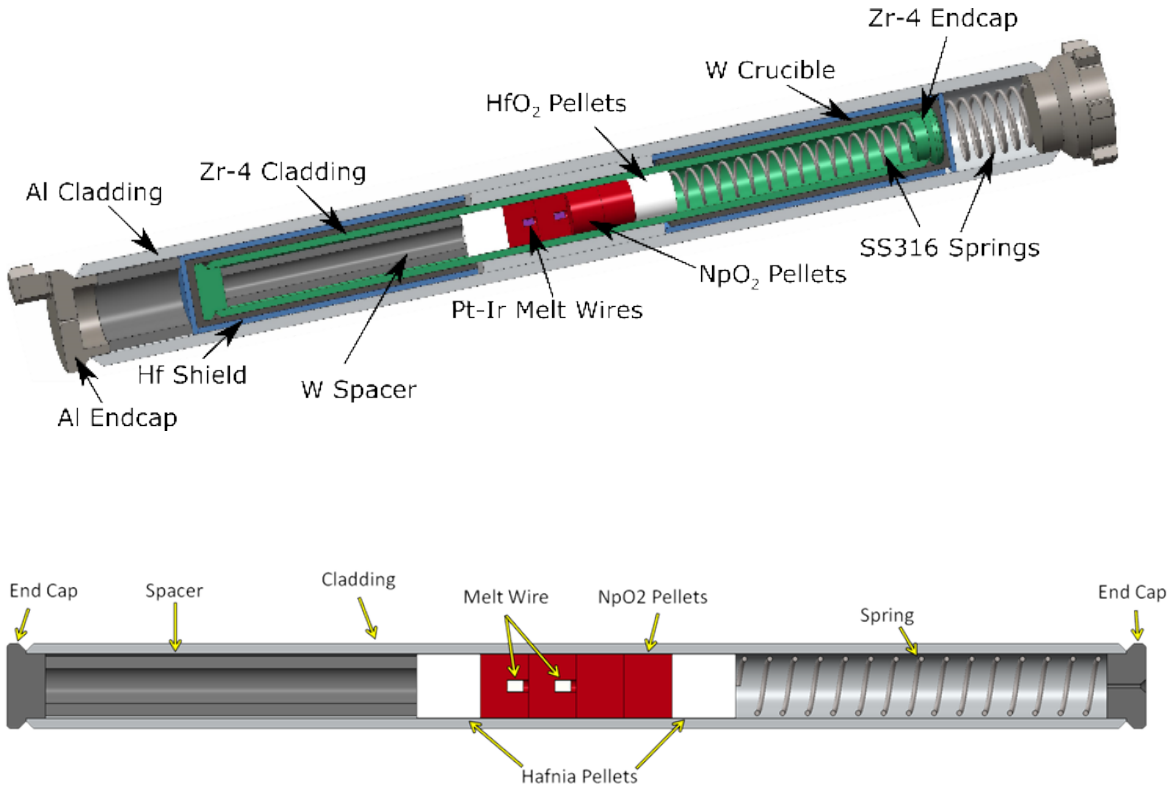

Figure 1. Cross section of target, tungsten end crucibles, and aluminum secondary capsule. The top illustration shows the entire assembly, target and secondary capsule, while the bottom shows only the target Note the melt wires in two of the pellets.

1.2 PELLETS

A key feature of the target design was the fabrication of high fraction of theoretical density [TD]) pellets. A neptunium nitrate solution underwent a modified direct denitration process, and after heating in air, the result is a NpO_2 powder suitable for pressing into a pellet.

1.3 TARGETS

Once the dimensions of the pellets were known, the pellets were grouped with the intent of minimizing variance in pellet outer diameter. The Zircaloy cladding's inner diameter was then reamed so that the pellet-clad gap was large enough to ensure reliable loading of the individual target while minimizing the heat transfer distance through the pellet-clad gas gap. The pellets were then loaded into the target, along with the other components and the end caps welded on; the targets were then pressurized with helium to local atmospheric pressure.

After the targets passed a leak check, they and the tungsten crucibles, hafnium shield, and supplementary components were loaded into the aluminum secondary capsules, and the end caps were welded on. The capsules were pressurized with helium to local atmospheric pressure and were then loaded into a basket assembly for insertion into HFIR.

2. IRRADIATION

2.1 MODELING ASSUMPTIONS

Because of uncertainties in the nuclear data, the irradiation design allowed for the possibility of pellet melting, and the secondary capsule and the tungsten crucibles were included.

2.2 HISTORY AND NEUTRON EXPOSURE

The targets were irradiated in HFIR for 2–4 cycles: cycles 477, 478, 479, and 480. Table 1 shows the targets and their cycles.

Table 1. The HFIR cycles to which each target was exposed

Capsule ID	HFIR location	HFIR cycle			
		477	478	479	480
NP01	VXF -01	✓	✓		
NP02	VXF -09	✓	✓	✓	
NP03	VXF -18	✓	✓	✓	
NP04	VXF -22	✓	✓	✓	✓

2.3 EXPECTED TEMPERATURES

High-fidelity coupled neutronics and depletion calculations were performed for the NpO_2 targets in HFIR to determine several key characteristics, including time- and spatially-dependent heat generation rates, ^{238}Pu yield, cumulative burnup, and fission product concentrations. These simulations were performed using the MCNP5 v1.5.1 for neutron/gamma transport calculations, SCALE 6.1.3 for depletion calculations, and ADVANTG 3.0.3 for variance reduction calculations. Additional code was written in Python 2.7 to facilitate communication between these software packages and parallelization of the simulations. NpO_2 targets were modeled for four 26-day HFIR cycles, and a 15-day decay period was assumed between cycles. Individual pellets were meshed into 10 radial and 8 azimuthal subsections of equal volumes to determine localized heat generation rates and isotopic concentrations. Time- and spatially-dependent heat generation rates were summarized and exported for use as inputs in follow-on finite element analysis (FEA) models of the experiment. Total fission gas (He, Kr, and Xe) production was also calculated for each time step of each HFIR cycle. Spatially averaged heat generation rates were between 70–74 W/g at the end of cycle 1, and the rates approached 115–123 W/g by the end of cycle 4. Peak heat generation rates reached 640 W/g in local subsections on the pellet surface at the end of cycle 4 due to the accumulation of fissile isotopes. Pellet burnup was estimated to be 36.9–39.5 MWD/kg by the end of cycle 4: this range was used to adjust thermophysical properties for the NpO_2 material. Models to illustrate burnup effects on thermal conductivity were extrapolated from models for mixed-oxide fuel as documented in the FRAPCON-3.0 code [3].

Three-dimensional FEA models of the experiment were solved in ANSYS 16.2 to determine component temperatures over four HFIR cycles. Fission gas release into the pellet-cladding gas gap was assumed to be 50% of total fission gas production for design conditions and 100% release for safety scenarios. Models for pellet densification, as well as pellet cracking and relocation, were taken from the FRAPCON-4.0 subroutines FUDENS and GTRLOC for UO_2 fuel [4]. A model for irradiation-induced swelling was taken from the FRAPCON-3.0 FSWELL subroutine and combined with the previously mentioned irradiation effects models to create a custom dynamic-link library (DLL) for the ANSYS model. This DLL uses the average pellet burnup and average linear heat rate (W/m) at any point in time to modify the

pellet's outer radius in accordance with the FRAPCON models. A heat transfer coefficient of 20.058 kW/m^2-°C and a bulk coolant temperature of 50.4 °C were calculated for design basis boundary conditions.

FEA models were solved for a range of conditions, including minimum, maximum, and nominal dimensional tolerances, as well as safety basis loss of coolant accident (LOCA) and flow channel blockage conditions. Average and maximum pellet temperatures at the end of 2, 3, and 4 cycles of irradiation assuming design basis conditions and nominal part dimensions are shown in Table 2. Iterations in the experiment design led to four slightly shorter NpO_2 pellets being irradiated instead of the original three pellets. Thermal modeling was performed using this three-pellet assembly and is representative of the four-pellet experiment since the pellet stack length, diameter, and mass are identical in both assemblies. The pellets are numbered according to their positions in the stack, with pellet 1 located below but closest to the HFIR midplane. Pellets 1 and 2 were expected to indicate localized melting after four cycles of irradiation. However, as previously mentioned, the thermophysical properties used in this modeling were extrapolations from models available in scientific literature, so they come with a moderate level of uncertainty. Results from the bounding safety basis conditions showed melting in all pellets after three cycles; however, additional analysis showed that this did not pose a safety risk to reactor operations due to the tungsten crucible and double containment design.

Table 2. Design temperatures (average | maximum °C) of NpO_2 target pellets at the EOCs 2, 3, and 4

Pellet	EOC 2	EOC 3	EOC 4	Melt temperature
Pellet 1	1606 | 2305	1824 | 2570	2027 | 2809	
Pellet 2	1659 | 2296	1870 | 2555	2065 | 2787	2706
Pellet 3	1528 | 2227	1735 | 2486	1921 | 2703	

EOC = end of cycle

3. POST IRRADIATION EXAMINATION

3.1 PIE PLAN

Five basic tasks were required for the post irradiation examination (PIE) of the NpO_2 pellet / Zircaloy capsule/target design:

1. *Cutting the capsule off the target pin by first cutting the capsule ends off and deburring the cut edges.* Next the capsule was turned vertical, and the components slid out. In one case, a push pin was needed to push the target out. Otherwise, no problems were encountered when removing the targets.

2. *Visual inspection of the target pin and the other capsule components to determine if there were signs of overheating.* Other than an uneven oxide layer on the targets, no signs of any heat-affected areas were noted on the targets' external surfaces.

3. *Milling a flat on the spring end of the target pin, thinning the wall down to about 0.030 in. so that the target clad can be punctured.* This was accomplished using an available in-cell milling machine without difficulty.

4. *Puncturing the targets and measuring the gas pressure in the target, the target free volume, and collecting the released ^{85}Kr using a cold trap system.*

5. *Segmenting the targets for MET and radiochemical samples.* Two MET mounts were desired from each target—one from the bottom middle, and one from the bottom—so that the melt wires could be examined. The remainder of the target material was used for radiochemical analysis.

Three general issues were of importance:

1. The general target performance (irradiation integrity) and the pellet swelling/shrinking/cracking/ melting behavior and fission gas release;

2. Any chemical and mechanical interactions between the pellets and the clad;

3. The ability to chemically process the pellets, recover the ^{238}Pu, recover and reuse the Np, and the ^{238}Pu yield and quality. This will be reported elsewhere.

A workflow diagram is shown in Figure 2. The PIE work was performed in Building 3525, and the radiochemical dissolution work was performed in Building 7920.

3.2 INITIAL RECEIPT OF THE TARGETS AND REMOVAL OF THE SECONDARY CAPSULE

The targets were loaded into the Building 3525 north hot cell bank and were briefly inspected for any damage; none was noted, and the targets appeared to be in good shape. An oxide layer (normal) was observed on the exterior of the aluminum capsules. A photo of the capsules is shown in Figure 3.

The aluminum capsule was removed by cutting the end(s) off with the in-cell Iso-Met saw and tapping/pushing the target out. See Figure 4. Note that the secondary capsule identification was clear and easy to read even through the hot cell window.

Figure 2. Diagram of PIE task flow and locations.

[1]SEM = scanning electron microscope
[2]IMGA = Irradiated Microsphere Gamma Analyzer

Figure 3. The four targets as received at Building 3525. Note the whitish oxide layer on the aluminum secondary capsules. Not shown in the picture is the NP01, NP02, NP03, and NP04 labeling etched on the aluminum.

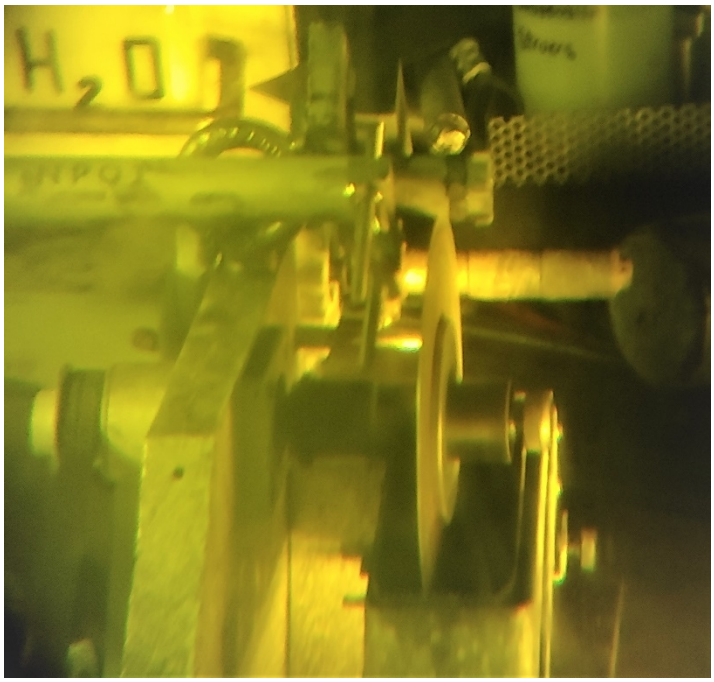

Figure 4. Cutting the end(s) off of the aluminum secondary capsule.
The label *NP01* can be clearly seen.

The targets were observed to have a presumed light oxide layer on them, with notably greater amounts of oxide on the ends of the targets, as shown in Figure 5.

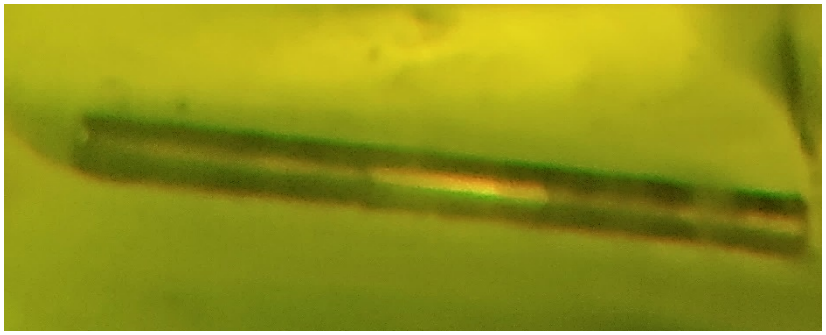

Figure 5. Target NP01 after removal from the aluminum secondary capsule. Other targets were very similar. Note the thicker, darker oxide layer on the ends of the capsule.

Other than the oxide layer, no other features of interest such as hot spots or damage were noted. Figure 6 shows that the target identification numbers are clearly visible.

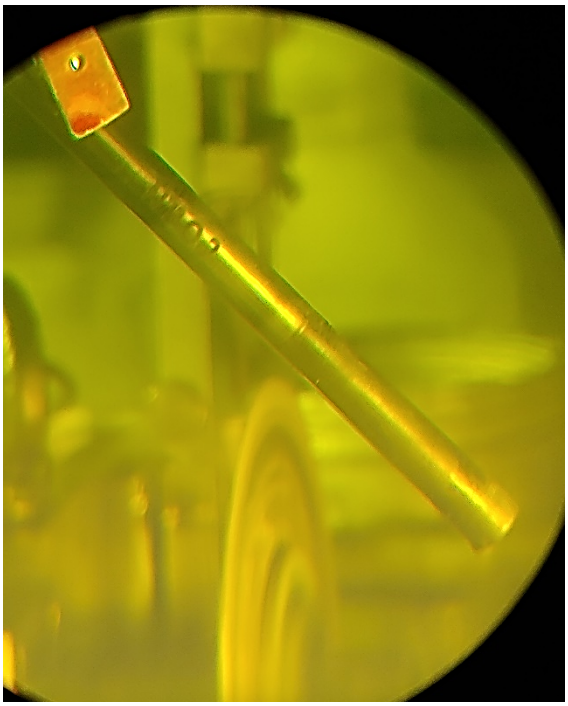

Figure 6. Target as removed from its capsule. Note the ID number on the target.

After the visual observation, a flat spot was milled on the targets to thin the cladding for the gas puncture task. Target NP01 was milled first and was punctured before the others were milled. Based on the results of this first puncture (see below), the flat spots on the other targets were made somewhat larger to accommodate any slight misalignment in the apparatus and to center the punch better in the milled flat region. A typical milling operation is shown in Figure 7.

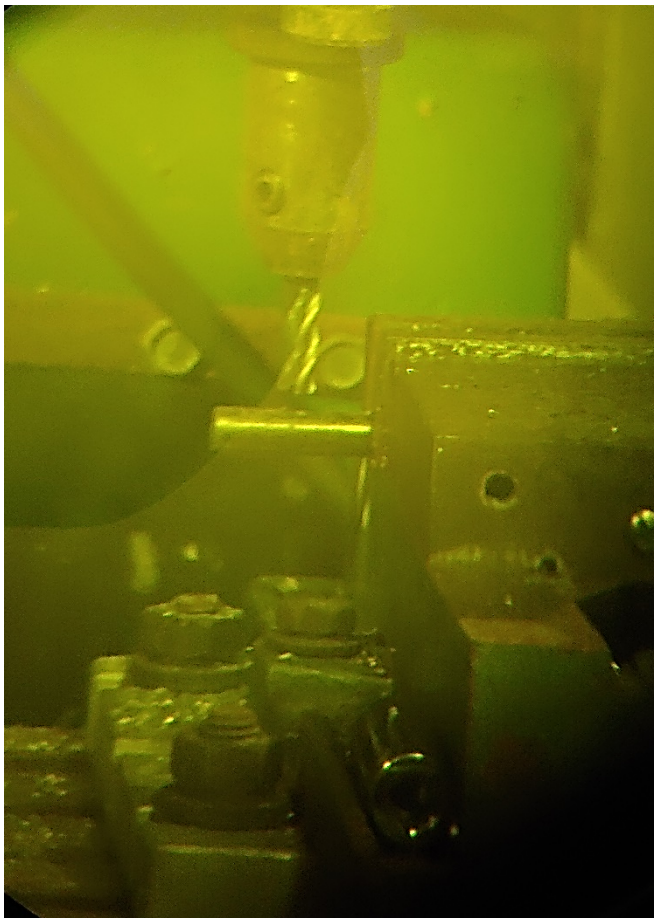

Figure 7. Milling the puncture flat on a target.

3.3 GAS PUNCTURE MEASUREMENTS

The target puncture task measured the target gas pressure and volume and collected the released ^{85}Kr. The schematic of the puncture system is shown in Figure 8, and an in-cell photo is shown in Figure 9. The system operation is documented in a formal procedure, and its operation is based on the ideal gas law. Briefly, the system is first pumped down to check for leaks, then the sample bottle (known reference volume) is used to compute the tare volume of the system by filling the bottle at a known pressure and measuring the final system pressure as it is discharged into the evacuated system; next, the system is pumped down again, and the selected target is punctured by turning the screw-driven puncture pin. The released gas pressure is then measured in the system, which is composed of the target internal volume and the system tare volume. Finally, and the system is brought up to slightly more than atmospheric pressure by the external helium source. Gas flow is then established through the system, which pushes the released gas through the cooled trap system, thus capturing the fission gases (^{85}Kr is of interest). After approximately an hour, the traps are removed and allowed to warm up. They are then gamma counted the first time, allowed to sit for several hours, and then recounted to investigate for reproducibility and/or leaks. Counting times are 1 to 6 hours; the longer 6-hour counting time provides the most reliable measurement of the trap inventory, whereas the shorter, 1-hour time shows whether the traps are free of activity prior to the test. Results from a final measurement of the target free gas volume and the tare volume are used to compute the target pressure; the target free volume can also be compared to the pre-irradiation value to check for consistency.

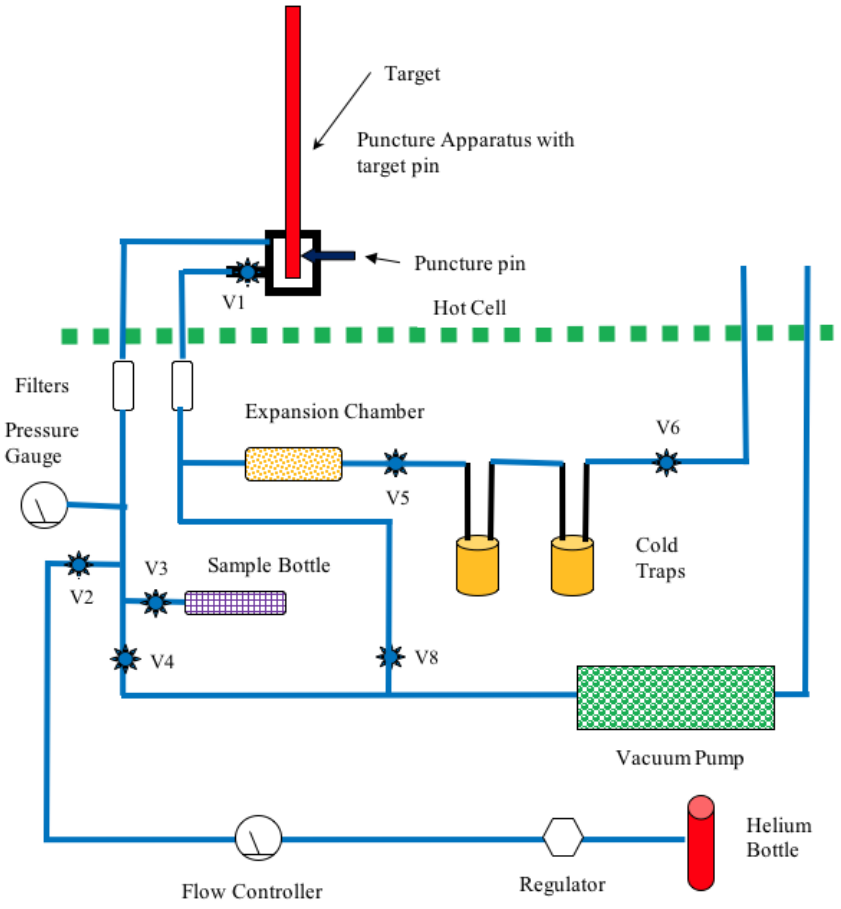

Figure 8. Schematic diagram of the target puncture apparatus.

Target NP01 was punctured first, and it appears that during the withdrawal of the puncture pin, some air may have entered the system; the process is sub-atmospheric (see Figure 10). After the puncture, a small misalignment of the milled flat and the puncture pin was observed. This resulted in the target being punctured just at the edge of flat, and more force was required than expected to turn the puncture pin. This exertion may have placed undue stress on the front seal, resulting in a momentary leak. The misalignment may have been caused by the weld seal bead on the top of the target, which was not accounted for when determining the position of the flat. To avoid this situation for the other targets, the flat was made larger to accommodate some misalignment. The other targets were milled after the NP01 puncture to allow for the improvement. The next target punctured was NP04, which did not require as much force on the punch pin. Its puncture history is shown in Figure 11. Note that there is only one pressure plateau (both targets had a pre-irradiation fill of atmospheric pressure). Finally, the remaining targets were punctured. The measured values are shown in Table 3.

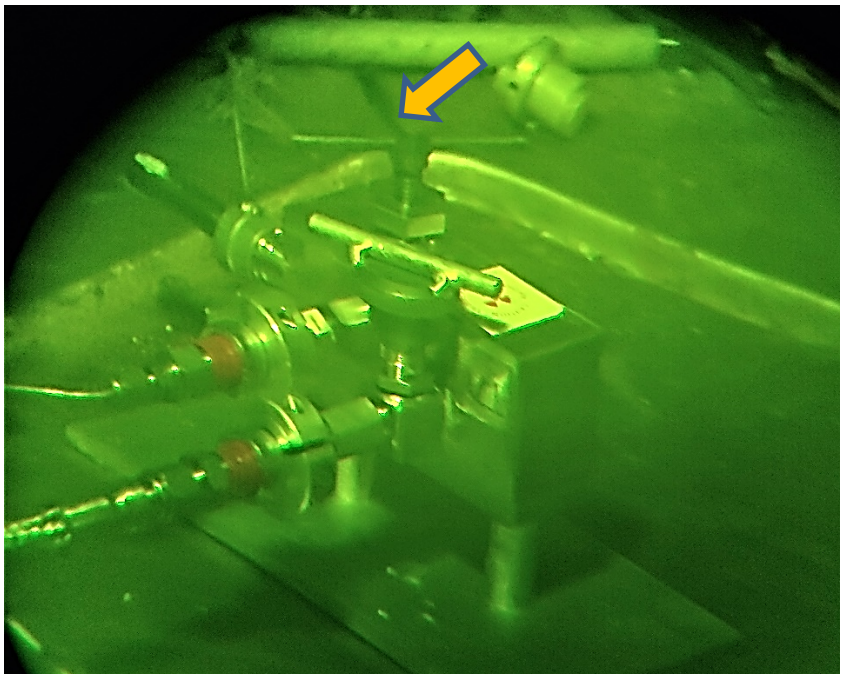

Figure 9. Target NP01 in puncture apparatus. The puncture pin is noted by the arrow. The target is projecting out from the left side.

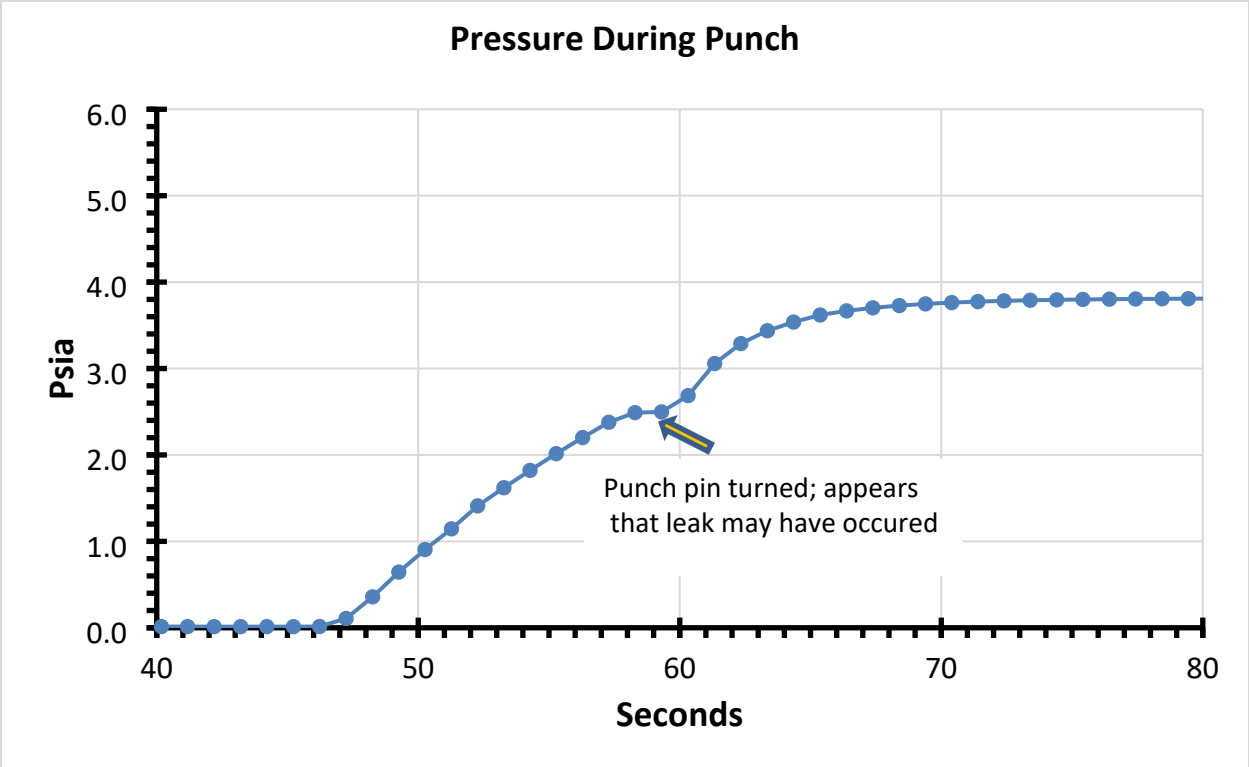

Figure 10. Pressure history during NP01 target puncture. Note the pressure plateau at 58 seconds; an air in-leak is suspected at 61 seconds.

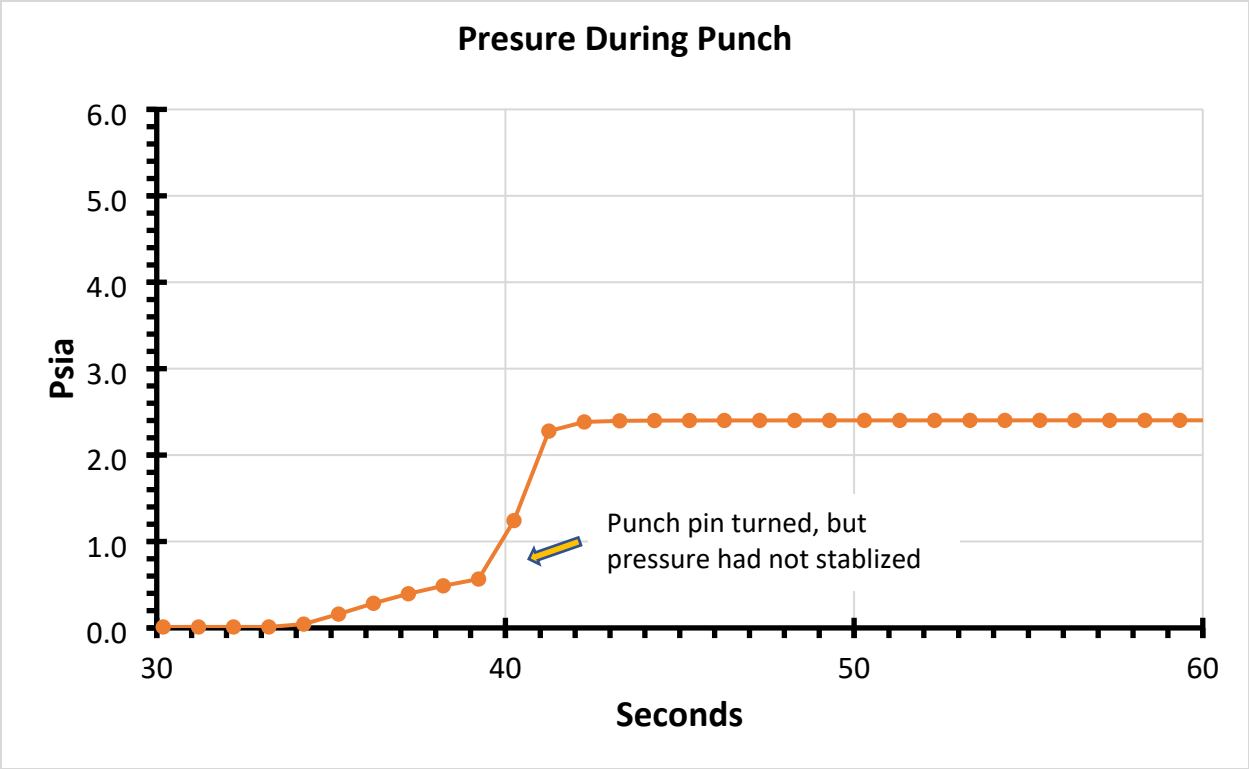

Figure 11. Pressure history for NP04. Note the single pressure plateau.

Table 3. Results of the target puncture (NP01 includes a pressure correction for a suspect leak just after the puncture, but it does not resolve the gas pressure problem. The ^{85}Kr measurement is independent and not affected.)

Parameter	NP01-Corr	NP02	NP03	NP04
Number of cycles	2	3	3	4
Release based on ^{85}Kr	3.8%	4.6%	38%	34%
Release based on gas g-mole	N/A	N/A	N/A	28%

Note: The g-moles measurement has high uncertainty unless the gas volume is large.

3.4 TARGET SEGMENTING

The targets were segmented into three specimens: an axial MET mount, a longitudinal MET mount, and a radiochemical specimen. A schematic of the cutting is shown in Figure 12. The schematic is based on the nominal drawing dimensions; the exact pellet boundaries may differ due to fabrication tolerances and radiation-induced dimensional changes. One objective for the target segmenting was to locate and examine the melt wires, which depends on the accurate location of the pellet boundaries and the integrity of the pellets once they have been cut.

A few hours after cutting, and prior to MET mount preparation, the axial sample for target NP01 crumbled into pieces and could not be mounted. To recover as much data as possible, the material was examined using an in-cell stereomicroscope to see if the melt wire could be located, but it was not found. However, examination revealed that the pellet had broken into small pieces and had not disintegrated into powder. There was no evidence of melting—the appearance was that of broken, consistent material. The

material had been loose in the cladding, so the pellet had not swelled enough to lock itself in place. The edges of the hole drilled to hold the melt wire were sharp, supporting the observation that the pellet had not melted. Figure 13, Figure 14, and Figure 15 show both sides of the cut specimen and the debris that fell out. Note that the appearance is consistent with that of a thermally shocked ceramic material.

The material for Mount NP01L was placed in a mount and potted in place, but in the process, the pellet also collapsed into a pile of debris that hardened in an irregular fashion. It was ground and polished as usual, but after processing, the only thing left was a portion of the hafnia pellet. Therefore, no useable mounts from NP01 were available for examination.

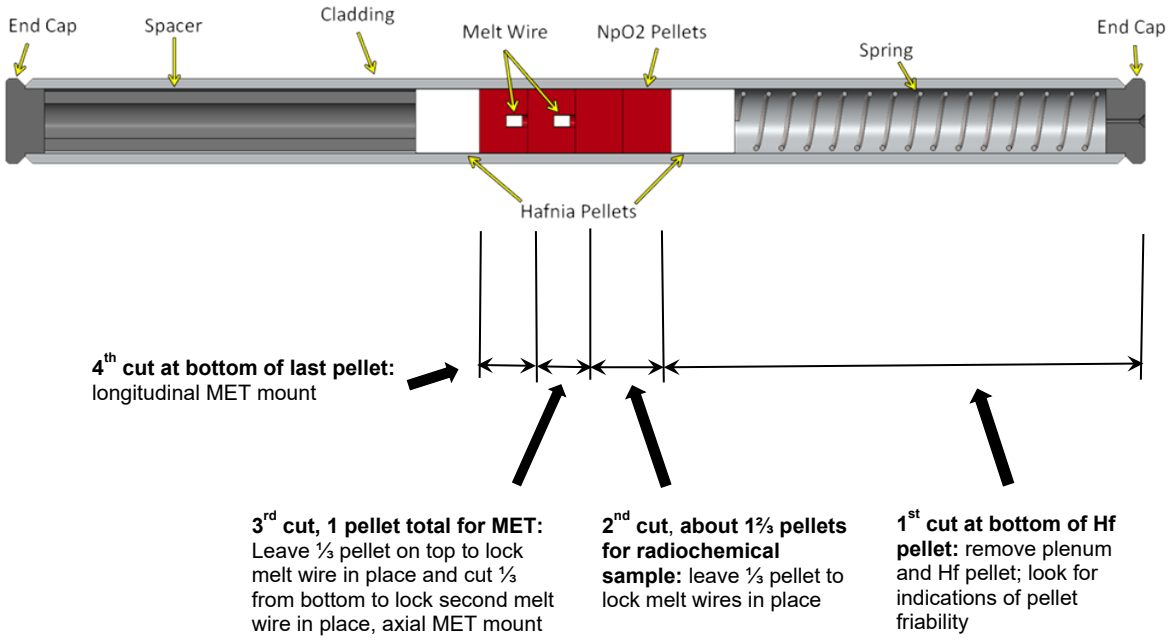

Figure 12. Nominal cutting locations for targets. One goal was to determine the state of the melt wires, so the cutting was conducted with this in mind.

The dispositions of the cut specimens are shown in Table 4. The cuts points in target NP03, which was that last specimen cut, were shifted slightly to try and better hit the desired locations after early feedback from grinding mount NP01L was evaluated. It was suspected that the pellet stack shrunk and/or the pellets shifted during cutting since they had not swelled enough to lock themselves against the cladding. The goal was to obtain a specimen that clearly showed the state of the melt wire(s) in a MET mount.

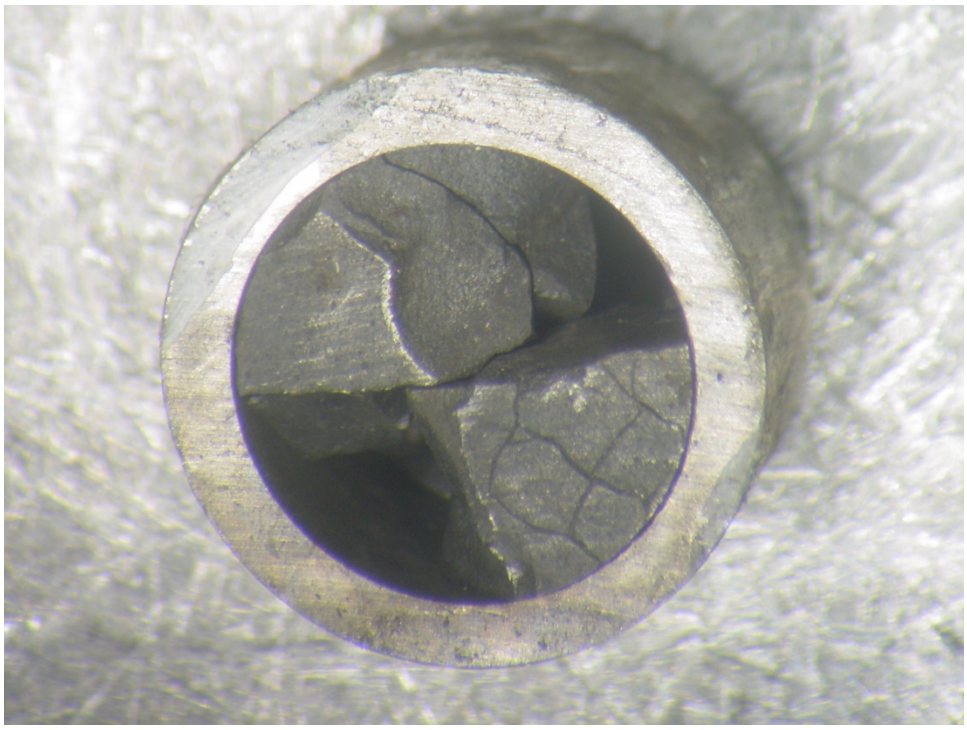

Figure 13. Bottom view of NP01 axial specimen.

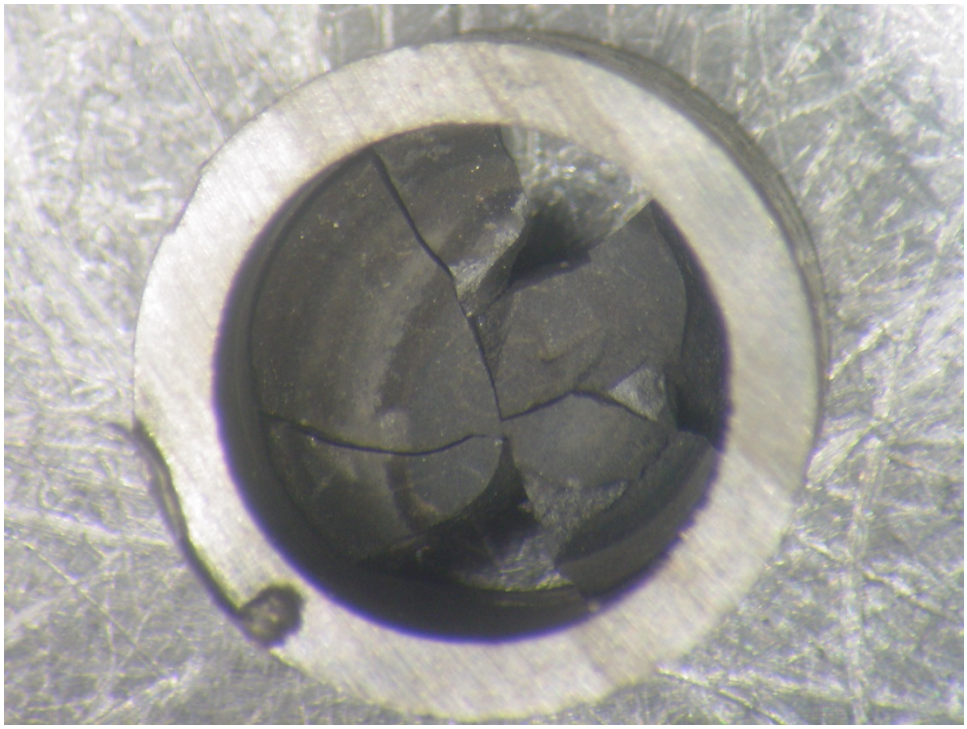

Figure 14. Top view of NP01 axial specimen.

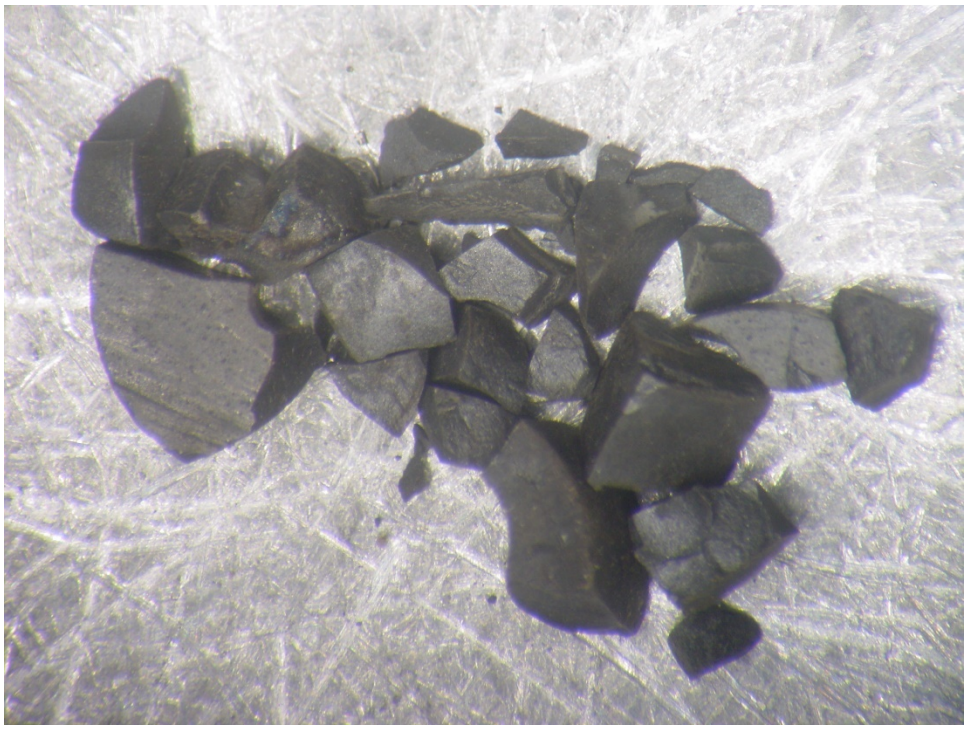

Figure 15. Debris from NP01 axial mount specimen. Note that the edges of the hole for the melt wire can seen in the large piece to the left of center. The melt wire could not be located.

3.5 MET RESULTS

The MET specimens were potted in phenolic mounts with epoxy glue. They were rough ground and re-potted with epoxy as necessary between grinding sessions to obtain a flat, low friability surface. They were then polished, cleaned, and photographed. The axial cross section NP04A is depicted in Figure 16, which shows some of the more extreme features of these mounts. Note that the small void in the lower left of the pellet appears to be the centroid of an off-pellet-center heat-affected region with cracks radiating outward. The source of the void is not clear; it may be a friable region that has come loose or perhaps a minor void formed from pore migration. There are no clear signs of melting. The material in the pellet rim region has a larger pore structure, consistent with assumed fabrication. Toward the heat-affected region, the porosity appears to be reduced and the density is increased, perhaps from additional sintering due to radiation and temperatures that were higher than the original sintering temperatures. Further toward the center, pore migration toward the centroid is apparent, with larger pores coalescing from migration of smaller pores. See Figure 17 for details. In addition, there is a gap between the pellet and the clad at room temperature, see Figure 16 for a sectional photograph. No pellet-clad interactions were noted; the clad's outer diameter is about 1.4% larger than the nominal fabrication pre-irradiated value. The target's internal and external pressures were low, so this change may have been due to material irradiation growth and a small amount of thermal creep.

Table 4. Target specimens

NP01 Component	*ID*	*Percentage of total (%)*	*Comment*
Entire target	NP01	100.0	
Radiochemical sample	NP01RC	40.7	Shipped to REDC for analysis
Axial MET mount	NP01A	25.2	Specimen crumbled into powder, repackaged with same name – no mount made
Longitudinal MET mount	NP01L	34.1	Specimen lost during mounting/grinding – friable mount did not pot in a useful manner
Scrap parts	NP01P	0.0	
Sum		***100.0%***	

NP04 Component	*ID*	*Percentage of total (%)*	*Comment*
Entire target	NP04	100.0	
Radiochemical sample	NP04RC	40.7	Shipped to REDC for analysis
Axial MET mount	NP04A	25.2	Successful mount
Longitudinal MET mount	NP04L	34.1	Successful mount
Scrap parts	NP04P	0.0	
Sum		***100.0%***	

NP02 Component	*ID*	*Percentage of total (%)*	*Comment*
Entire target	NP02	100.0	
Radiochemical sample	NP02RC	40.7	Shipped to REDC for analysis
Axial MET mount	NP02A	25.2	Successful mount
Longitudinal MET mount	NP02L	34.1	Successful mount
Scrap parts	NP02P	0.0	
Sum		***100.0%***	

NP03 Component	*ID*	*Percentage of total (%)*	*Comment*
Entire target	NP03	100.0	Shortened to compensate for possible shrinkage based on early MET work
Radiochemical sample	NP03RC	40.6	Shipped to REDC for analysis
Axial MET mount	NP03A	24.9	Successful mount
Longitudinal MET mount	NP03L	34.5	Successful mount
Scrap parts	NP03P	0.0	
Sum		***100.0%***	

The longitudinal mount NP04L is shown in Figure 18. Part of the hafnium pellet was captured due to a small misalignment from either the pellet stack slipping or shrinking. Cutting of NP03 was adjusted in an effort to eliminate this problem. The region to the left of the axial center line appears to have the heat-affected zone structure, which may be related to the heat-affected region detailed above, although the orientation of the pellet is not known. Note the extensive cracking in the NpO_2 pellet, whereas there is much less cracking in the hafnium pellet (top). Also note that a gap can be seen between the pellet and the clad, and the pellet end just below the hafnia pellet is relatively flat; it is not grossly bulged or swelled out. Thus, at this level of radiation exposure, the pellets are suffering few serious radiation-induced gross dimensional effects other than thermally induced cracking.

In contrast to NP04, NP02 showed less structure in central regions of the pellet; however, the heat-affected zone is still present. The axial mount NP02A is shown in Figure 19. Here, the heat-affected zone is less visible, and cracking is typical. Unfortunately, the center area where the melt wire was expected to be was damaged by pull-out. The pellet-gap can be seen in Figure 19; the average value is somewhat smaller than for mount NP04A. The inner and outer clad measurements are also shown in Figure 19; the outer diameter is 0.5% larger than the nominal fabrication value. The outer diameter of the 3 cycle mounts are important, as they show that little clad deformation occurred during irradiation for the period of most interest. Finally, the longitudinal mount NP02L is shown in Figure 20. This particular mount suffered extensive cracking. The bottom of the pellet also appears to be nearly flat, with no strong swelling behavior.

The axial cross section mount NP03A is shown in Figure 21; the heat-affected region and cracking are similar to that of NP02A, but the region appears to be somewhat larger, and like NP02A, the central region is affected by pull-out and the likely loss of the melt wire during handling. The NP03A pellet-gap can be seen in Figure 21; the average value is close to that of NP02A and is smaller than that of NP04A. The outer diameter is 1.0% larger than the nominal fabrication value. Less cracking and relocation is apparent in the longitudinal mount NP03L, possibly due to a better cut location. As seen in Figure 22, there is a gap between the pellet and the clad and the rather flat pellet bottom at the junction between the two pellets. All the mounts show no significant pellet swelling, with the existence of a small gap between the pellet and clad, probably due to minor pellet densification.

A summary of the target OD changes is shown in Table 5. A high-contrast comparison of the two 3-cycle mounts, NP02A and NP03A, is shown in Figure 23. Note that the heat-affected area appears to be larger in mount NP03A, which was the 3-cycle mount with the much greater fission gas release. There is no clear reason for this difference, as both targets were assumed to be irradiated under the same conditions. Further investigation of irradiation conditions is needed to provide further information. Figure 24 compares NP03A to NP04A; they appear to be more similar than NP02A and NP03A.

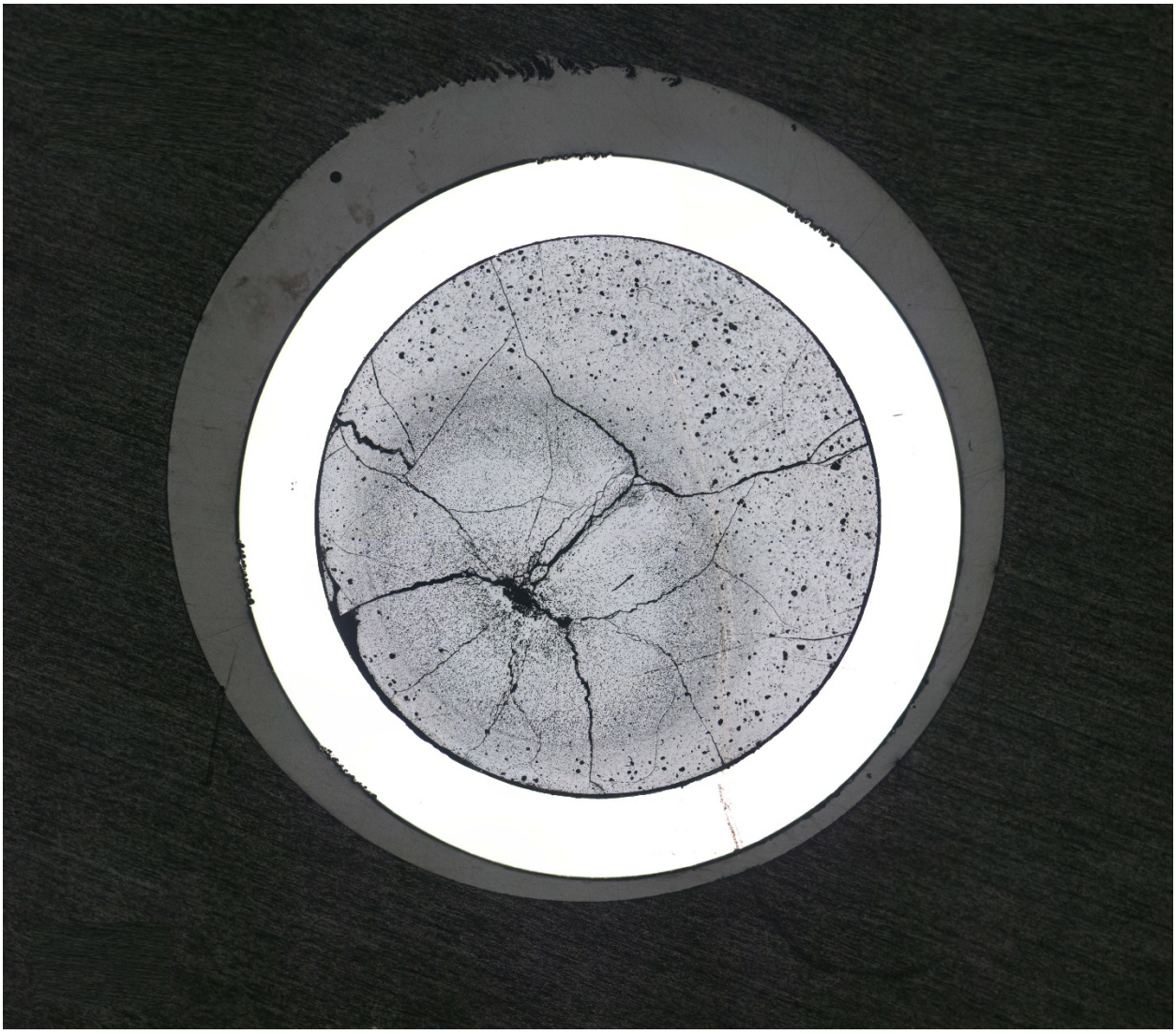

Figure 16. Mount NP04A.A heat effect zone is evident in the lower left of the photo. It appears that the small void is near the zone center, from which cracks are radiating. A change in porosity can be seen from the pellet's edge to the zone center, as well as a gap between the pellet and the clad.

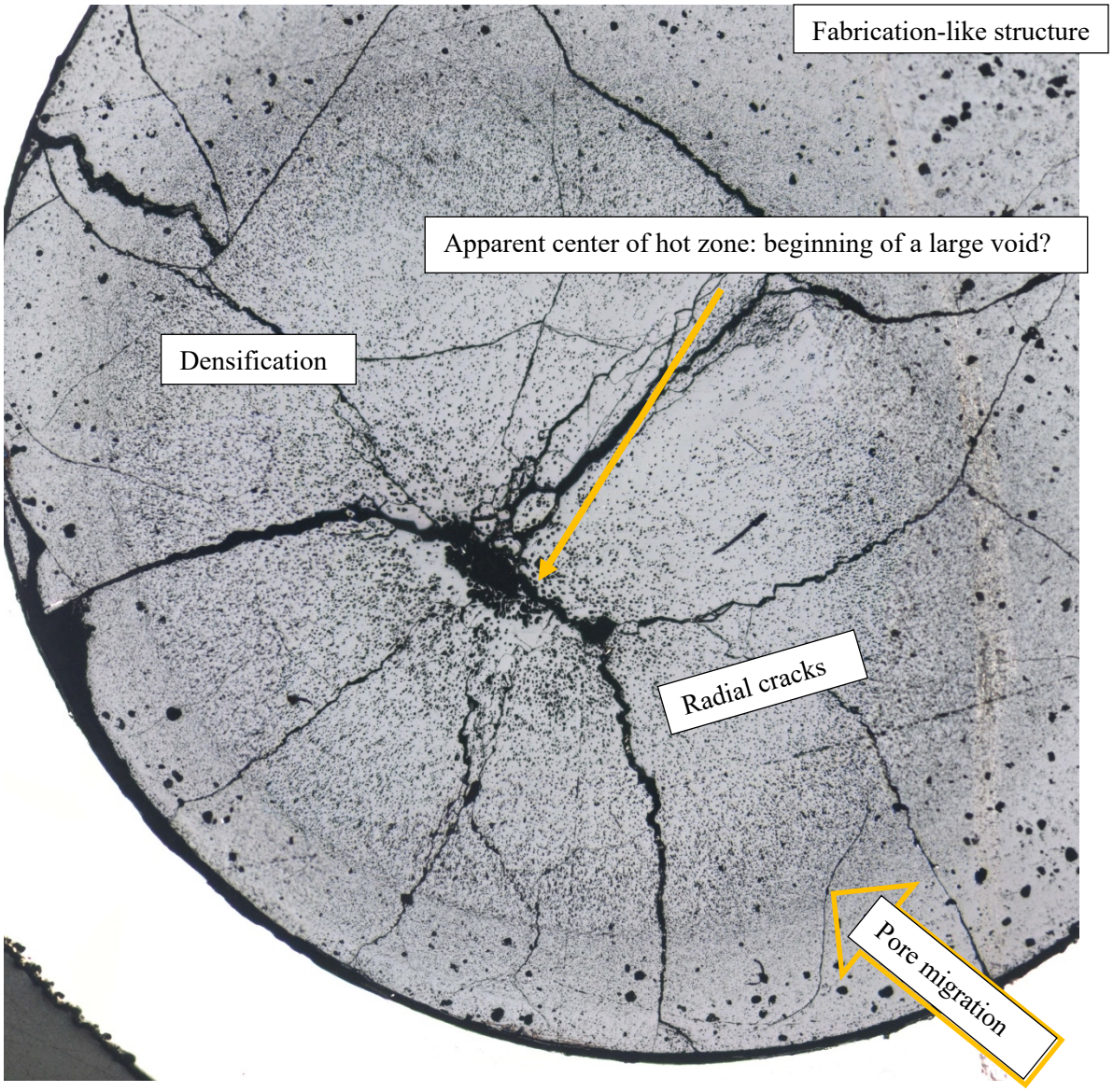

Figure 17. Enlarged heat-affected region in NP04A. Note the pore migration and change in structure from the pellet's edge to the void. No melting is apparent, although pore migration is an indication of high temperatures, which were suspected to be >1,700 °C.

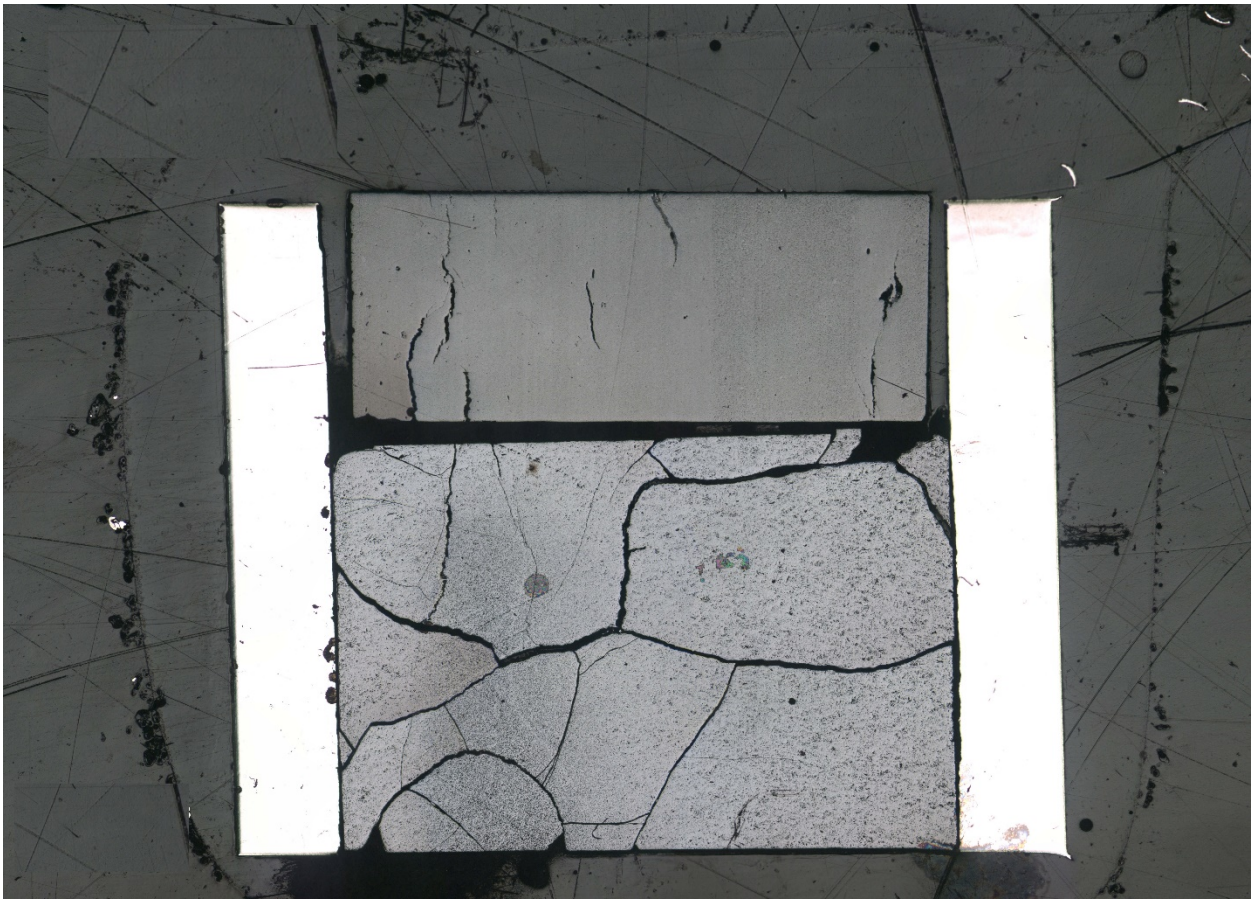

Figure 18. Mount NP04L. The top pellet is a portion of the hafnia pellet, and the lower cracked pellet is the NpO_2 pellet. Either the cutting was slightly off, or the pellet stack moved or shrank enough to affect the cutting plans; thus, the inclusion of a portion of the hafnia pellet. Note the cracks in the NpO_2 pellet. There appears to be less porosity to the left of the axial center of the NpO_2 pellet. It is not known whether this aligns with the heat-affected zone. This mount was ground down to near, but not exactly center.

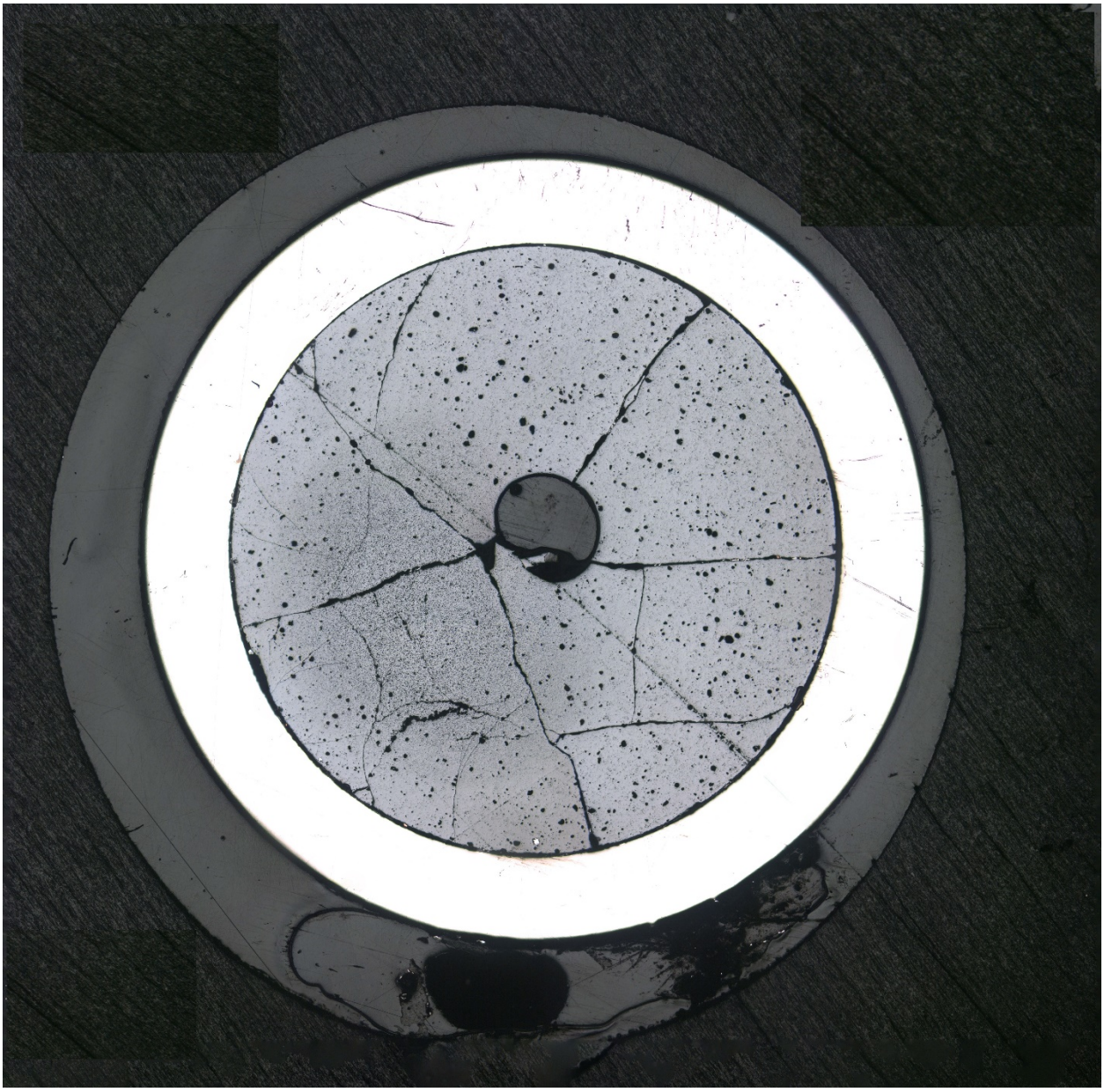

Figure 19. Mount NP02A. The heat-affected zone is in the lower portion of the photo, just left of center, and it is much less notable than that shown in NP04A. The black region in the center is epoxy in a pull-out region; unfortunately, this is where the melt wire was expected to be.

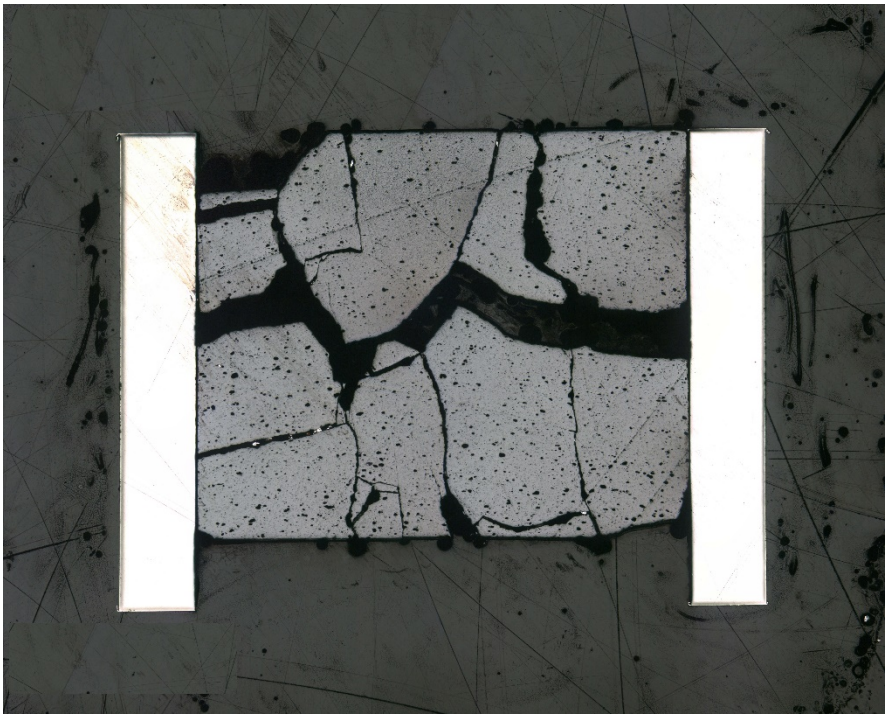

Figure 20. Longitudinal mount NP02L. This mount suffered extensive cracking, but there appears to be no deleterious behavior of the pellet or clad. This mount was ground down to near, but not exactly center.

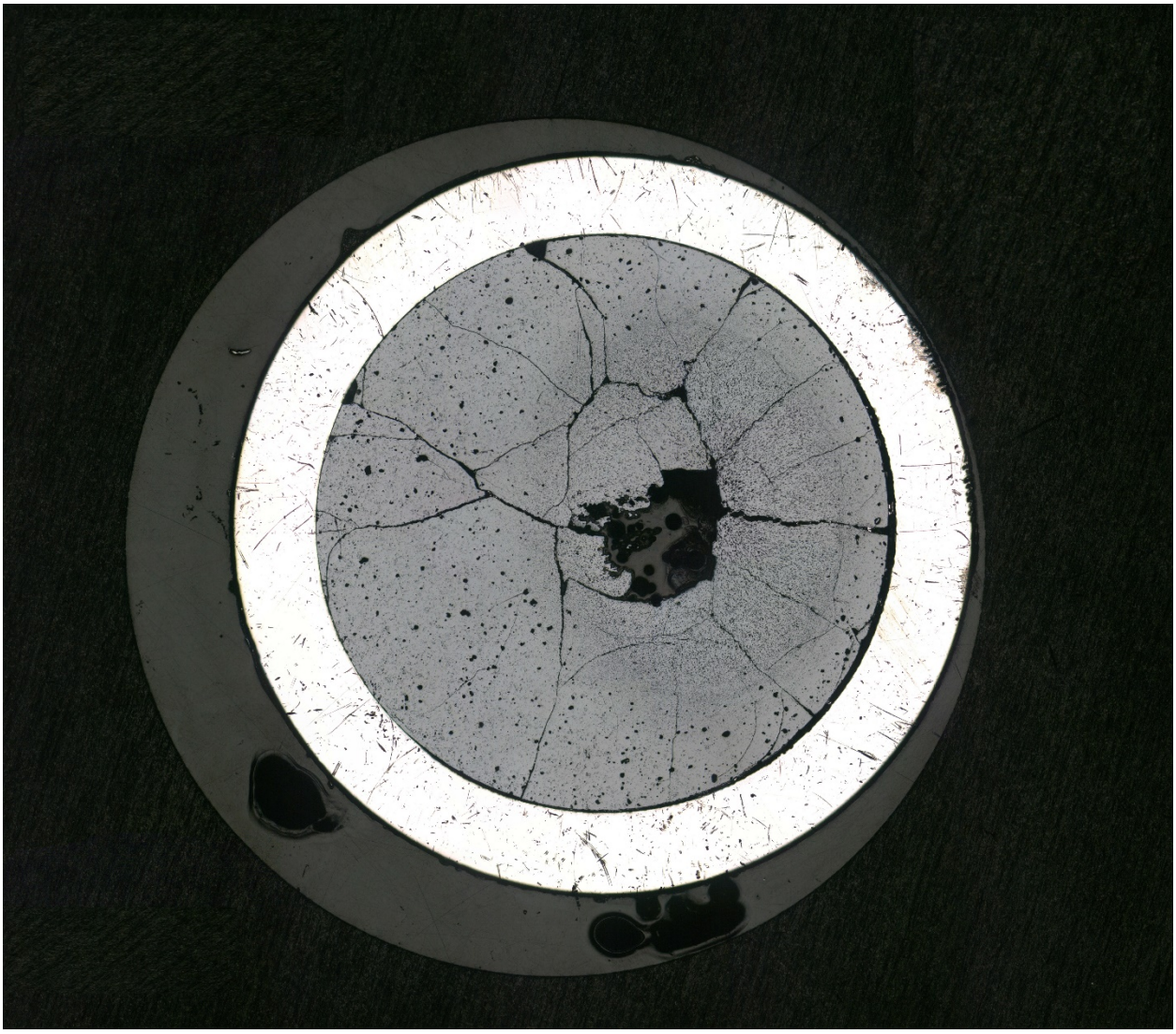

Figure 21. Mount NP03A. The heat-affected zone is in the right half of the image. It is similar to that of NP02A, but larger in area. Unfortunately, a large pull-out area obscures a portion of the heat-affected zone, which is also where the melt wire was expected to be.

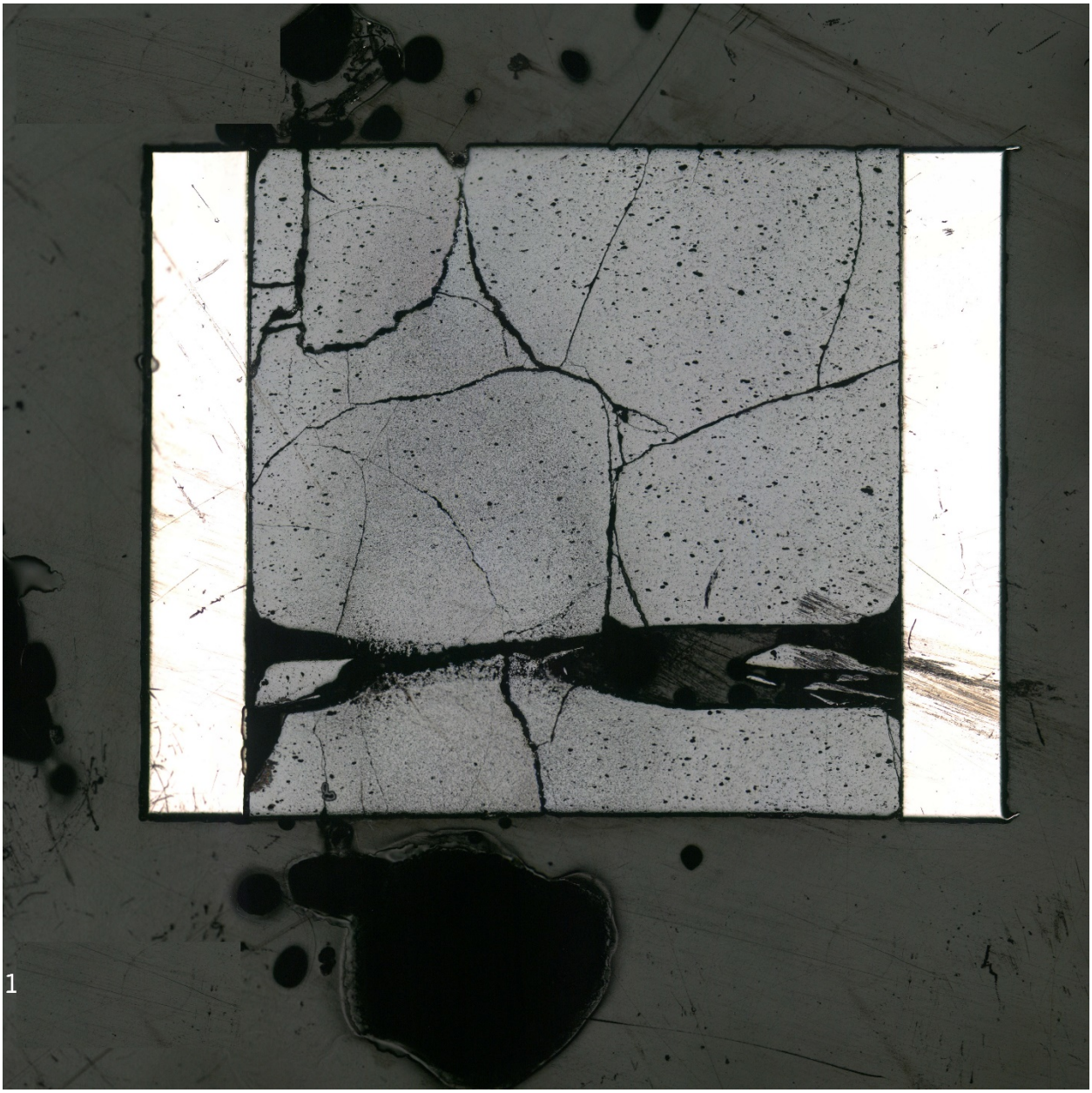

Figure 22. Longitudinal mount NP03L. This mount is similar to the others, except there is less cracking. This mount was cut from a slightly different location in an effort to avoid the difficulties with the other mounts. This image captures the junction between two pellets; the melt wire was expected to be at the bottom end of the upper pellet. It was either ground through or was not exposed. The left side of the image (small pores) may show some of the heat-affected zone. No deleterious pellet or clad behavior is apparent. This mount was ground down to near, but not exactly center.

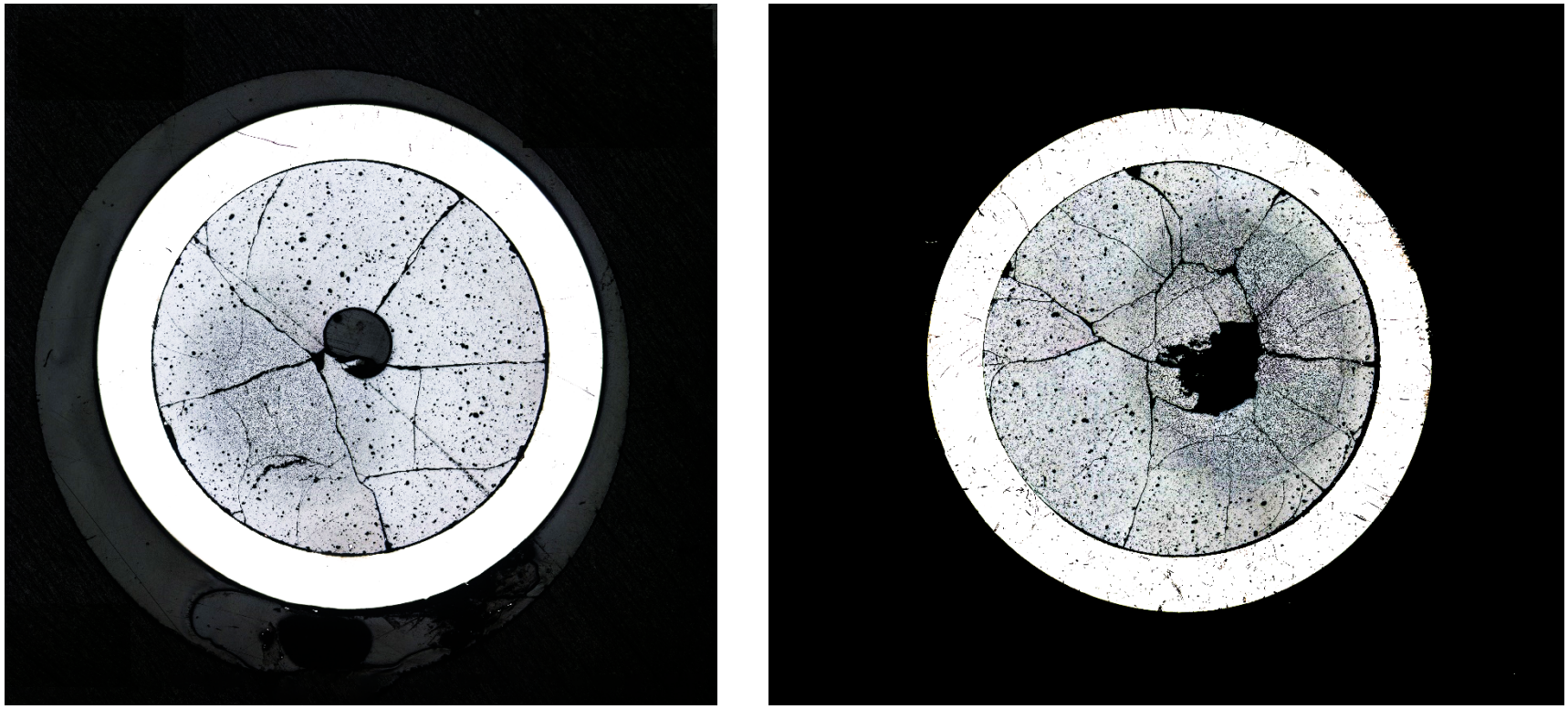

NP02A **NP03A**

Figure 23. High-contrast comparison of the two 3-cycle pellet mounts. Note that NP03A on the right appears to have a larger heat-affected zone. This target also had a much higher fission gas release. It is not clear whether this is an exposure effect or a temperature effect.

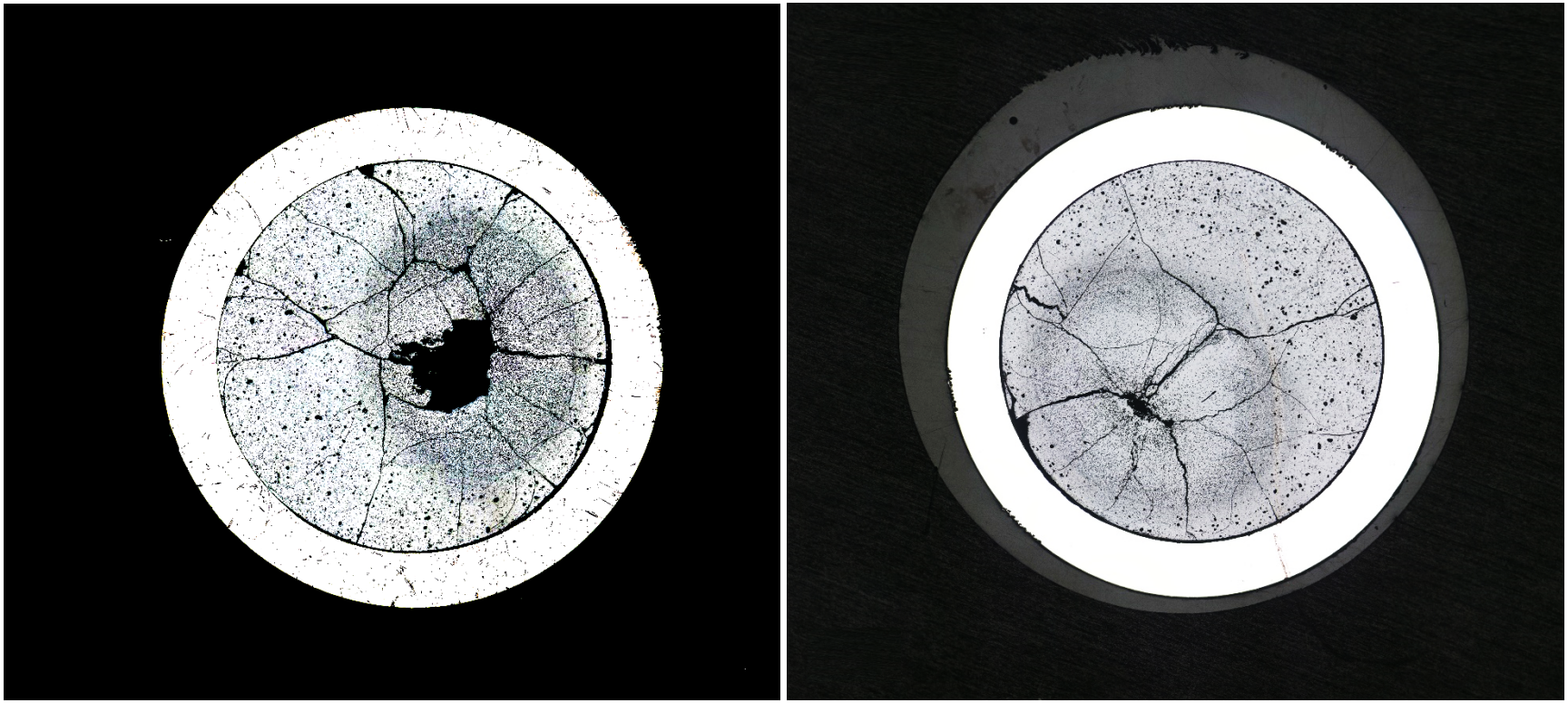

NP03A **NP04A**

Figure 24. High-contrast comparison of NP03A (3-cycle) and NP04A (4-cycle) pellet mounts. Note that they are much more alike than the pair of 3-cycle pellet mounts shown in Figure 23.

Table 5. Clad diameter changes

Mount	Number of cycles	OD percent change
NP02A	3	0.5%
NP03A	3	1.0%
NP04A	4	1.4%

3.6 RADIOCHEMISTRY RESULTS

The amount of ^{238}Pu produced in the targets is shown in Table 6 along with their previously reported gas release. These results are shown in graphical form in Figure 25. Note that the average of the three cycle results would place the targets on a fairly linear trend with irradiation cycles. Complete details are in Appendix A-1.

An attempt was made to grid down Mount NP02A very thin (to minimize dose) so an SEM/Microprobe analysis of the Pu distribution along the cross section of the pellet could be made, but the high friability of pellet made this impossible; the mount crumbed before it could be properly polished for the instrument.

Table 6. Radiochemical results

Target	Irradiation cycles	^{238}Pu mg/g pellet	^{85}Kr percent release
NP01	2	40.6	3.8%
NP02	3	53.1	4.6%
NP03	3	59.1	38%
NP04	4	72.9	34%

3.7 DISCUSSION & CONCLUSIONS

The behavior seen in the MET mounts is typical of that expected for a dense oxide that has been irradiated and temperature cycled. These pellets were quite friable, and they easily broke up into small pieces during handling and polishing, resulting in less-than-desirable polishing. However, usable MET mounts were obtained that could be used to examine the pellet structure after irradiation. Two features were of importance. First, the off-center power peaking and its greatest effect on the 4-cycle target was observed and could be easily contrasted with the 3-cycle irradiation targets. Second, as predicted, the pellets did not swell into the cladding and permanently strain it. A pellet-clad gap was observed in both the 3- and 4-cycle targets and was inferred in the 2-cycle target based on the fact that it fell apart.

The fission gas release was somewhat confusing. As expected, the 2-cycle target had the lowest release at 3.8%, and the 4-cycle target had a high release at 34%. However, one of the 3-cycle targets had a low release of 4.6%, and one had a high release of 38%. One possible explanation for the low fission gas release in the 3-cycle target could be related to how the assembly was oriented in the reactor. As mentioned in Section 1.1, a highly absorbing, semicircular hafnium component was included in the assembly to simulate the neutron flux suppression from having multiple NpO_2 pins behind the front-facing pin in a production target—facing away from the HFIR core. If the experiment were installed backwards with the hafnium component facing the HFIR core, then the neutron flux would be suppressed over the course of irradiation, resulting in less fission gas production and less heat. However, it is difficult to retrospectively determine the actual orientation of the target, and the Pu production was comparable to

that of NP03. The average of these two values is 21%, which is more typical. ^{238}Pu production appears to be largely linear with irradiation cycles, as expected.

Overall, no deleterious effects were noted that would threaten the concept or that would create difficult irradiation conditions. The major issue to watch is the fission gas, release as it may be sensitive to some unknown fabrication or irradiation conditions.

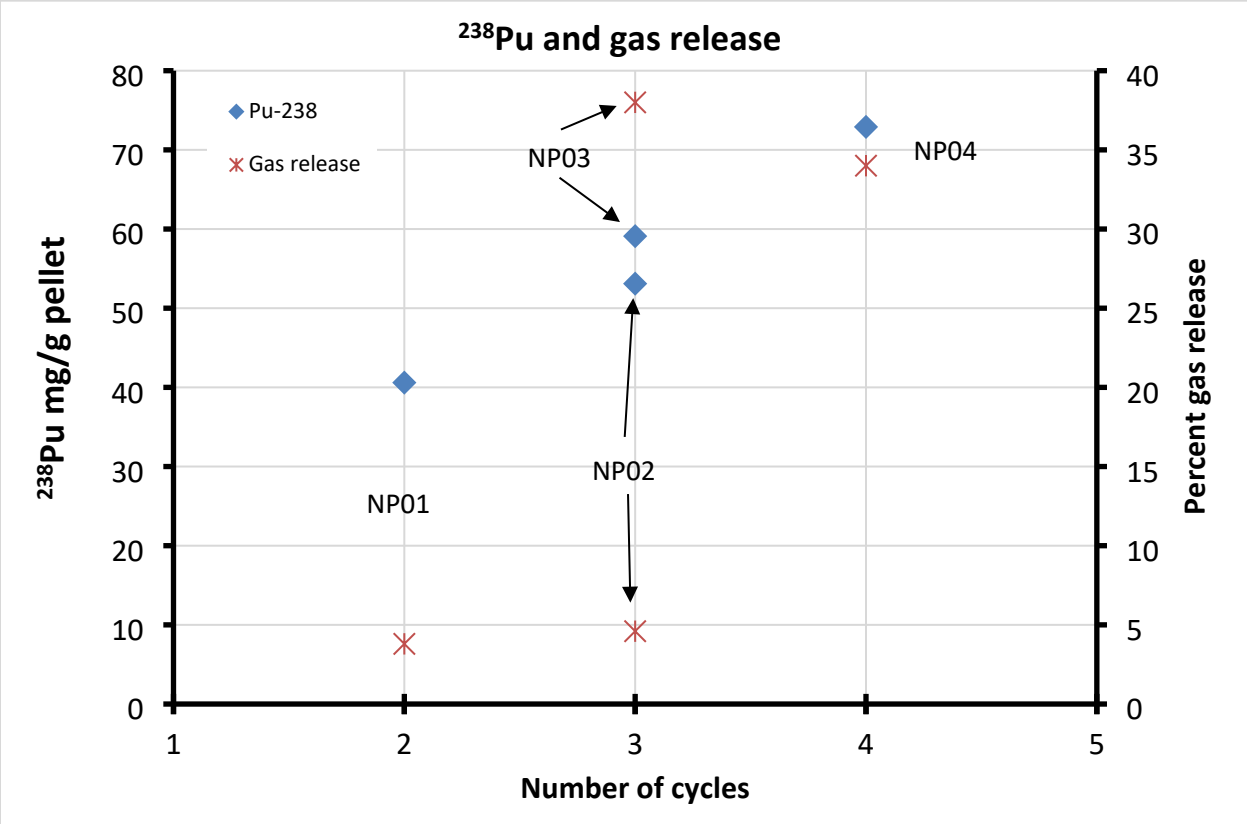

Figure 25. ^{238}Pu and gas release versus irradiation cycles.

4. ACKNOWLEDGMENTS

The authors wish to thank Robert Wham for the program post-irradiation examination (PIE) support, Jerid Metcalf and the support staff at Building 3525 for their help and effort in performing the many in-cell PIE tasks, Joel McDuffee for supporting the capsule and neutronic analysis, Jeffrey Delashmitt and the staff at the Radiochemical Engineering Development Center (REDC) for the radiochemical analysis, Emory Collins for the ^{238}Pu systems analysis, and Rose Raney and Kathy Jones for support with document preparation.

5. REFERENCES

1. R. M. Wham, L. K. Felker, E. D. Collins, D. E. Benker, R. S. Owens, R. W. Hobbs, D. Chandler, and R. J. Vedder, *Reestablishing the Supply of Plutonium-238*, The American Institute of Aeronautics and Astronautics Propulsion Energy (AIAA 2015), Orlando, FL, July 2015.

2. R. J. Vedder, *Preparation of Sintered $^{237}NpO_2$ Pellets for Irradiation to Produce ^{238}Pu Oxide*, ORNL/TM-2017/728, September 2018

3. Lanning, D., C. Beyer, and C. Painter, *FRAPCON-3: Modifications to Fuel Rod Material Properties and Performance Models for High-Burnup Application.* NUREG/CR-6534, Vol 1, PNNL-11513, 1997.

4. Geelhood, K.J., W.G. Luscher, P.A. Raynaud, and I.E. Porter, Pacific Northwest National Laboratory, *FRAPCON-4.0: A Computer Code for the Calculation of Steady-State, Thermal-Mechanical Behavior of Oxide Fuel Rods for High Burnup*. PNNL-19418, Vol. 1 Rev. 2, 2015.

APPENDIX A.

The results of the target radiochemical and mass analyses are shown in Table A.1.

Table A.1. Radiochemical analyses results

Target number	NP01	NP02	NP03	NP04	Average 01 & 04	Average 02 & 03
Number of HFIR cycles	2	3	3	4	3	3
Activity						
Alpha PHA 5.50 Mev, Bq/g sample	2.49E+10	3.40E+10	3.70E+10	4.39E+10	3.44E+10	3.55E+10
^{238}Pu, Ci/g sample	0.673	0.919	1.00	1.19	0.930	0.960
^{238}Pu, mg/g sample	39.1	53.4	58.1	69.2	54.1	55.8
ICPMS						
^{238}Pu, mg/g sample	40.6	53.1	59.1	72.9	56.8	56.1
Total Pu, mg/g sample	43.4	58.0	65.1	81.9	62.2	61.6
Np, mg/g sample	794	794	751	789	792	773
Np/^{238}Pu ratio	19.6	15.0	12.7	10.8	13.9	13.9
Np/total Pu ratio	18.3	13.7	11.5	9.6	12.7	12.6
Pu isotopic analysis, %						
^{238}Pu	93.48	91.50	90.73	89.01	91.25	91.12
^{239}Pu	6.02	7.75	8.39	9.76	7.89	8.07
^{240}Pu	0.41	0.67	0.78	1.08	0.75	0.73
^{241}Pu	0.07	0.064	0.09	0.14	0.11	0.08
^{242}Pu	<0.02	0.007	0.01	<0.02	<0.02	0.009
Gamma spec, Ci/g sample at reactor discharge						
^{95}Zr	0.935	0.909	1.09	1.435	1.01	1.00
^{144}Ce	0.188	0.263	0.342	0.373	0.281	0.303
^{106}Ru	0.087	0.116	0.113	0.142	0.115	0.115
^{134}Cs	6.90E-04	1.50E-03	1.64E-03	2.30E-03	1.50E-03	1.60E-03
^{137}Cs	7.20E-03	1.13E-02	1.16E-02	1.35E-02	1.04E-02	1.15E-02
^{155}Eu	5.30E-04	6.10E-04	9.70E-04	1.03E-03	7.80E-04	7.90E-04

A parameter of major interest is the time required to dissolve the pellets. As noted in the main document, the pellets fragmented into many pieces, but not into fine dust. Thus, the dissolution started out with a fair amount of surface area, which was of benefit. The dissolution time for a 4-cycle pellet is shown in Figure A-1. The dissolved fraction is compared to that from the calculations, and an additional amount of nitric acid was added at the 100-hour point. The temperature was held near the solution boiling point of 105–120°C, depending on solution acid concentration.

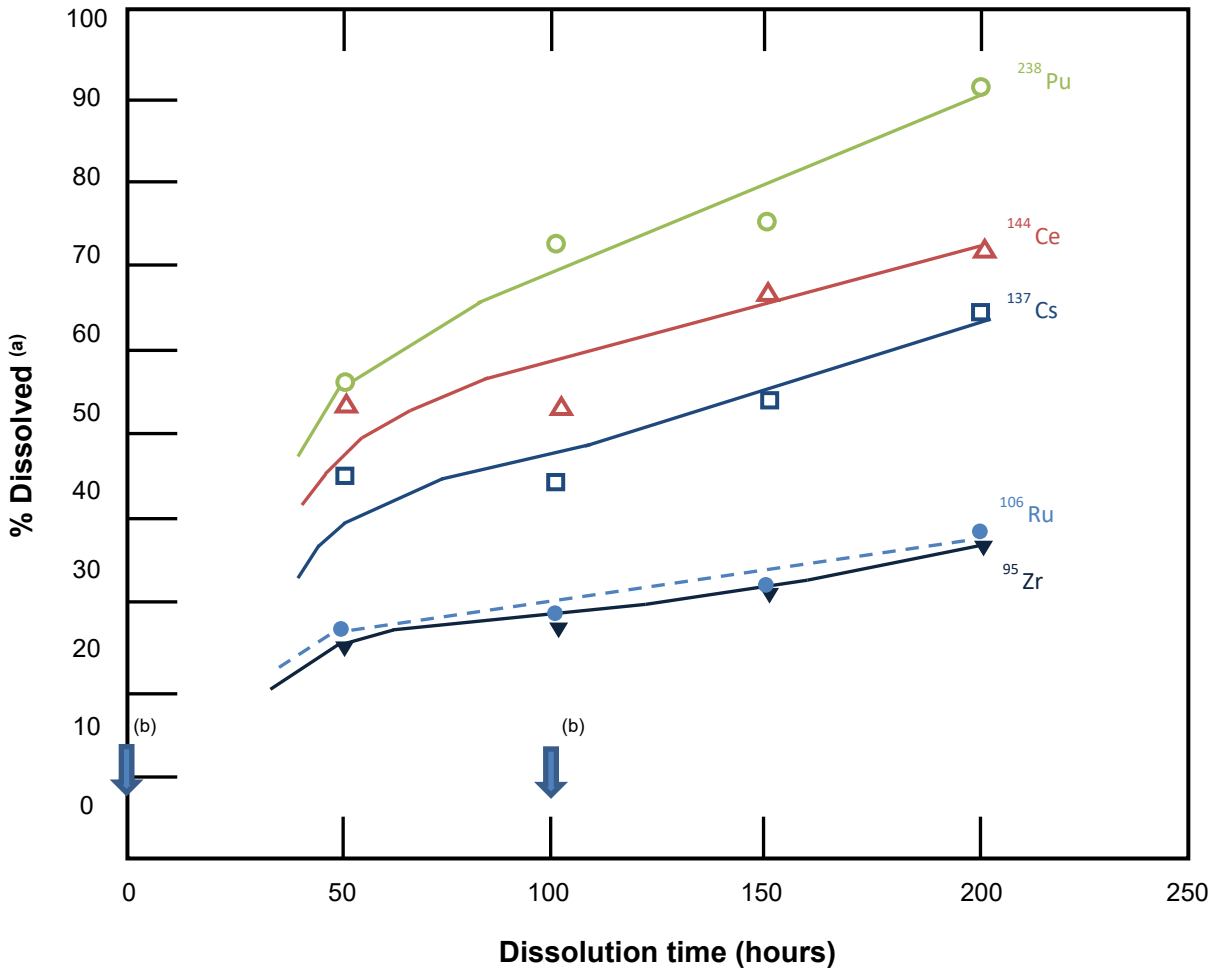

Figure A.1. Isotope dissolution rates of HFIR 4-cycle irradiated test target pellet in nitric acid without hydrogen fluoride. (a) Based on total predicted by ORIGEN, (b) 50 mL 12M HNO_3 initial dissolvent; 10 mL concentrated HNO_3 added after 100 hours.